Uncertainty and conceptual model of a camera system in a car crash test scenario

Timo Kaminski[1], Sören Vogel[2], Karsten Raguse[1], Ingo Neumann[2], Hamza Alkhatib[2]

[1] Volkswagen Aktiengesellschaft, Vehicle Safety, 38436 Wolfsburg, Germany - (timo.kaminski1, karsten.raguse)@volkswagen.de
[2] Geodetic Institute, Leibniz Universität Hannover, Germany - (vogel, neumann, alkhatib)@gih.uni-hannover.de

Keywords: Uncertainty Modeling, Crash-Test Validation, Monte Carlo Simulation, Dynamic Measurements, Bootstrapping

Abstract

Accurately estimating injury severity in crashes relies on understanding vehicle occupant movements. This is simulated using crash test dummies in controlled test cases. Currently, stationary high-speed cameras positioned outside the vehicle track the kinematics of the different dummy parts by following optical markers placed on these dummies. However, onboard high-speed cameras are primarily used for documentation and are not suitable for determining 3d object kinematics with the required accuracy. Furthermore, with the increasing sophistication of modern airbag systems, points inside the vehicle that need to be visible for the stationary cameras may be obscured by the deployment of airbags. To address this limitations, we propose relocating onboard high-speed cameras inside the vehicle and investigating the resulting uncertainties. The dynamic nature of crash events presents challenges for these onboard cameras to accurately self-localize, given the rapid changes occurring within the vehicle. To overcome this challenge, we introduce a novel method for determining the position and orientation of the onboard stereo camera pair at each time point, followed by an analysis of the uncertainties involved. We use Monte Carlo simulations and bootstrapping techniques to estimate the uncertainties associated with point measurements in crash test scenarios. And therefore we can determine the object kinematics and their related uncertainties inside the vehicle using the onboard high-speed cameras instead of the stationary high-speed cameras.

1. Introduction

Road traffic accidents remain a leading cause of injury and fatality worldwide, underscoring the critical importance of enhancing occupant protection systems. To mitigate the risks associated with collisions, automotive manufacturers invest heavily in optimizing vehicle structures and restraint systems, such as seat belts and airbags. These optimizations are tested and validated through controlled crash tests, which are essential for assessing the performance of safety features under realistic impact scenarios.

High-speed cameras are used in crash tests to assess impact dynamics. They are usually positioned to the side or suspended from the ceiling. The cameras are calibrated to focus on optical markers placed on the vehicle bodywork and within the interior, including those on crash test dummies. However, the effectiveness of this approach is challenged by the increasing use of advanced airbag systems. While the deployment of additional and larger airbags, such as curtain and center airbags, enhances occupant protection, it often results in occlusions that obscure interior points. This obstruction impedes the ability to accurately track marker movement, thereby hindering the validation of crash simulations. To circumvent these occlusions, methods such as the deactivation of individual airbag areas or the removal of parts of the bodywork have been employed. However, these procedures add costs, risk damaging the vehicle structure, and may not always be effective. Alternative approaches include using MEMS inertial sensors (Björkholm et al., 2010) and X-ray imaging during safety tests (Leost et al., 2020), (Butz et al., 2021). Zhang et al. (Zhang et al., 2022) proposed a system utilizing interconnected cameras and checkerboard patterns for localization, enhanced by inertial sensors and extended Kalman filters. This method is promising, even if the area of application is limited. The entire floor should be provided with a checkerboard pattern and the system is also very susceptible to vibrations due to its lever arm.

To address these challenges and close the existing research gap, we propose an improved stereo camera system to be installed onboard. This system is designed to function throughout the crash event, even when movement extends beyond predefined patterns. The core idea is that at least one camera localizes itself based on the exterior environment using bundle adjustment, allowing for accurate positioning without relying on interior reference points that may become occluded or move during the crash. This outward-facing camera is permanently linked to another camera viewing the interior, ensuring that their relative orientation to each other is pre-calibrated and therefore known and that this camera-to-camera orientation is stable within the crash test. The system is designed so that their fields of view do not overlap.

Our primary objective is to achieve a level of three-dimensional point uncertainty comparable to that of existing stereo systems, with a maximum permissible deviation of less than 5 mm in each spatial direction (Raguse and Heipke, 2009). To estimate and validate this level of accuracy theoretically, we conduct an uncertainty analysis using bootstrapping (Efron, 1979) and Monte Carlo (MC) simulation. The MC method (Metropolis and Ulam, 1949) allows us to model the probabilistic behavior of the system under various configurations, providing a comprehensive estimate of measurement uncertainties.

In this paper, we present the development and evaluation of the above-mentioned onboard stereo camera system for crash tests. We examine various configurations, discuss their advantages and disadvantages, and address the associated uncertainties. This advancement is crucial for validating crash simulations and ultimately enhancing vehicle safety.

The content of this paper is organized as follows: In Section 2, the methodology of the proposed system is described in detail, including the setup and computational processes. Section 3 presents the results of the uncertainty analysis, which was conducted using MC simulations and bootstrapping. In Section 4, we analyze the implications of our findings and evaluate them in comparison with existing methods. Finally, Section 5 provides a conclusion to the paper and outlines potential future research.

2. Methodology

In the following chapter, two different configuration proposals are presented as possible solutions: a system with three cameras and another with four cameras. The uncertainty of the point measurements with the systems is estimated using MC simulation. This requires the inclusion of uncertainties related to system calibration and localization through image measurements. The uncertainty of localization using linking images is estimated by bootstrapping (Efron, 1979).

2.1 Overview of the Proposed Camera Systems

Due to the abrupt deceleration during a crash, the vehicle's position and orientation change relative to the world coordinate system. This sudden movement generates vibrations, which also affect the mounted cameras directly on the vehicle. These vibrations are unpredictable and depend, for example, on the type of crash test, the vehicle type, and the mounting of the camera in the interior. As a result, movement and orientation cannot be reliably predicted.
The basic idea is to install two cameras together which have a fixed orientation between each other during the crash. The images recorded by the system are precisely synchronized in time during the test with an accuracy of less than 20 µs. One camera looks outwards, the other inwards. The camera facing outwards combines the recorded images using bundle adjustment. The result of the bundle adjustment is the translation and orientation in the world coordinate system of the camera pointing outwards in each epoch. By pre-calibrating the translation and orientation of the two cameras in relation to each other, the orientation and translation of the inward-facing camera can be derived. This system fulfills the requirement for the kinematic analysis if the view to the outside is permanently unobstructed. The system is shown in Figure 1.

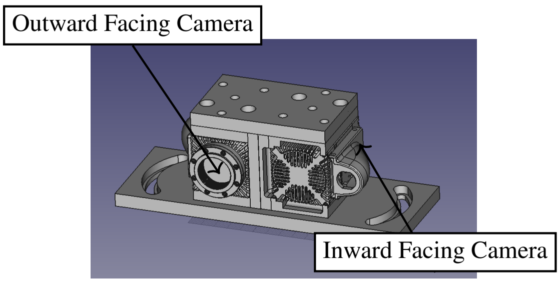

Figure 1. CrashCamMINI 3530 Pair without objective

Four camera system In the initial test configuration, each camera positioned within the interior is accompanied by an additional camera. This configuration ensures the independence of the base between the cameras, eliminating the necessity for scale measurement. The configuration has the advantage that the camera poses are independent of each other. There is nearly no correlation between the poses of the camera pairs. Refer to Figure 2 for a schematic illustration.

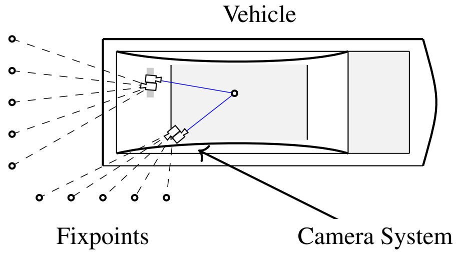

Figure 2. The overview sketch provides a top-down perspective of a vehicle equipped with integrated camera systems. The system is capable of directly measuring a point in space.

Three camera system In the second experimental setup, a pair of cameras along with an additional single camera is utilized. The outward-facing camera of the pair aligns itself using the fixed environment as a reference and transfers the pose to the inward-facing camera. An additional camera located within the vehicle is connected based on tie points with the relative orientation in each epoch. To determine the scale of the base, a scale is measured in each epoch. This scale must be within the field of view and must not deform during the crash. The advantage of this solution is that it reduces the number of cameras needed; however, the uncertainties of the point measurements may be larger. Figure 3 provides a schematic representation of the setup.

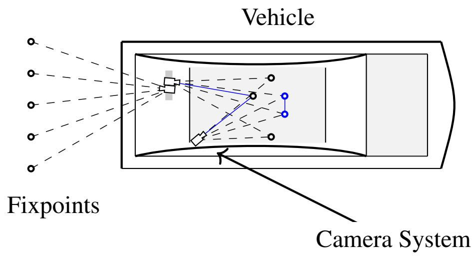

Figure 3. The overview sketch provides a top-down perspective of a vehicle equipped with integrated camera systems. The direction of view to points is indicated by dashed lines, and the connected blue dots represent the scale for measurement.

2.2 Camera Calibration and Configuration

To determine the alignment between the cameras, we need to consider six degrees of freedom. Calibration involves aligning the projection centers of both cameras and determining their relative positions and orientations. The positions of the cameras' projection centers depend on the sensor, lens characteristics and how they are mounted. The base (i.e., the separation between cameras) depends on how the cameras are installed relative to each other. Since we cannot directly infer the projection centers from housing measurements, the base and orientation must be calibrated using images. To maintain calibration during the crash, the cameras are connected by metal plates directly mounted on their housings. The lenses are screwed into the threads and then glued to ensure they remain firmly connected. We use two CrashCamMINI 3530 cameras from Imaging Solutions GmbH. An illustration of the system is provided in Figure 1
The calibration process requires two steps. First, the internal

orientation of each camera must be established using test field calibration. Next, the camera pair is moved through all degrees of freedom in a laboratory setting, as illustrated in Figure 4.

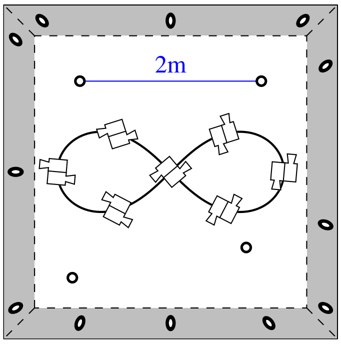

Figure 4. The Z and Y planes are shown from a top-down perspective. The walls with circular markers are indicated in grey, and the scale is shown in blue. The camera pair moves along the black trajectory.

In the laboratory, markers are installed that serve two purposes: they act as reference points between components and provide a calibrated scale of 2 meters in length. Using a large scale reduces the base uncertainties. The images are then analyzed using a bundle adjustment with elliptical markers and SIFT feature points. After the bundle adjustment, the 3D coordinates of the markers are exported. The scaling factor can be calculated using the exported marker points on the scale. In each epoch, when both images are included in the bundle, the base and orientation between the cameras can be calculated as follows:

$$\mathbf{H}_{\text{cam1}}^{\text{cam2}} = \mathbf{H}_{\text{cam1}}^{\text{init}} \cdot \left(\mathbf{H}_{\text{cam2}}^{\text{init}}\right)^{-1} \qquad \mathbf{H} = \begin{bmatrix} \mathbf{R} & \mathbf{t} \\ \mathbf{0} & 1 \end{bmatrix} \tag{1}$$

Where $\mathbf{H}$ is the Homography between two systems, e.g. the initial system and the system of cam 1 and/or cam 2, the Homography $\mathbf{H}$ consists of the Rotation $\mathbf{R}$ and the translation $\mathbf{t}$ between the two systems. The scale is fixed and set to 1. The mean values from the entire data set are used for calibration. As the number of observations n increases, the standard deviation of the calibration roughly decreases proportionally to $1/\sqrt{n}$. The standard deviation is given by $\sigma_{\text{calibration}} = \frac{\sigma}{\sqrt{n}}$. This calibration allows us to estimate the standard deviation associated with a single measurement, corresponding to the standard deviation computed from all measurements.

2.3 Uncertainty Analysis Techniques

The overall uncertainty is influenced by multiple factors, including the uncertainty of the outward-facing camera, the calibration uncertainty between cameras, uncertainties arising from linking additional cameras through image matching, and uncertainties related to pixel measurements and system configuration. To estimate the uncertainty of the image-based localization, we employ bootstrapping. Monte Carlo simulations are then used to integrate and quantify the combined uncertainties.

2.3.1 Bootstrapping The bootstrapping technique is a powerful statistical resampling method introduced by Efron in 1979. It estimates the distribution of a statistic by sampling with replacement from the original data, enabling the derivation of confidence intervals and uncertainty measures without making strict assumptions about the underlying distribution. In the context of our camera system, bootstrapping is employed to estimate the uncertainty of camera poses, particularly when direct derivation of covariance matrices is impractical.
The bootstrapping technique works by resampling the dataset of image matches, generating multiple new datasets from the original. For each new dataset, we calculate camera poses using bundle adjustment or relative orientation techniques, deriving a statistical distribution of these poses. The repeated resampling provides insight into the variability and reliability of the camera pose estimates. This approach is particularly advantageous for estimating uncertainties in scenarios where occlusions or image quality might limit the effectiveness of traditional covariance analysis.

Flowchart Bootstrapping Matches To estimate the uncertainty in the absolute orientation the six degrees of freedom (6DoF) between two images without using an external sensor, we perform the process multiple times. In each iteration, we randomly select the same number of matches from the total set of image feature matches and generate a new dataset. Each dataset may contain duplicate matches due to the resampling process. We then calculate the absolute orientation based on the new dataset, aligning the images to a fixed coordinate system. The poses from each iteration are recorded for further analysis. The procedure is illustrated in flowchart from in Fig. 5. This method ensures that variations in scaling are taken into account, as the points used for alignment may differ across iterations, providing a robust estimate of uncertainty across different configurations.

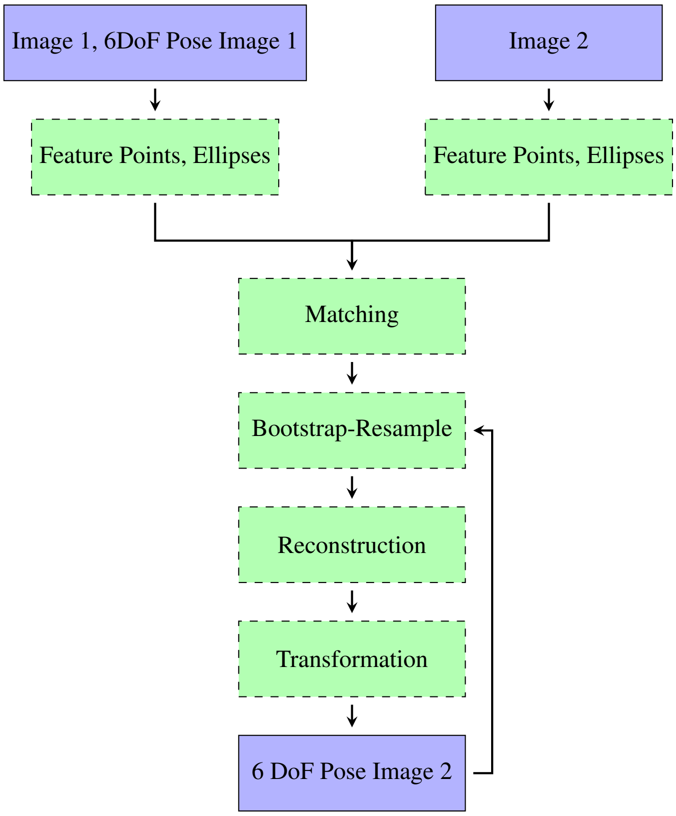

Figure 5. For reasons of simplicity, the flowchart model refers to two images. The bootstrapping samples are drawn from the complete matching set. The six parameters of the pose are then determined iteratively.

The bootstrapping technique provides a robust estimate of uncertainty that accounts for potential variations in image matching, ensuring that the system's performance remains reliable even under less-than-ideal conditions. It also allows us to quantify how sensitive the camera system is to errors in image feature matching, providing critical insights for improving system design and robustness.

2.3.2 Monte Carlo Simulation We employ the Monte Carlo simulation method, as described by Metropolis and Ulam 1949, to estimate the uncertainty in photogrammetric point measurements. Monte Carlo simulations are particularly valuable for propagating uncertainties through a complex system, allowing us to understand the probabilistic impact of various sources of error on the final results.

The uncertainty in point measurement depends on the uncertainties associated with the cameras, which arise from factors such as camera calibration, image matching, and sensor noise. These uncertainties are determined either directly– such as through bundle adjustment – or indirectly by linking the camera to another using image matching. The goal of the Monte Carlo simulation in this context is to quantify how these uncertainties influence the accuracy and reliability of the final 3D spatial measurements. To accurately propagate uncertainty from one camera to another, we need to account for the six pose parameters (three for translation and three for rotation) and their associated standard deviations. Additionally, calibration or absolute orientation parameters for each camera have uncertainties that must be incorporated.

Monte Carlo simulation involves generating multiple random realizations of these uncertainties and applying them to estimate their cumulative effect on the system. Specifically, homogeneous transformation matrices are used to represent the relative positions and orientations of the cameras, and random variations are introduced based on known standard deviations. The following pseudocode outlines the procedure for propagating uncertainties through a camera pair.

Uncertainty Propagation Camera Pair

Input: $\mathbf{H}_{\text{init}}^{\text{cam1}}, \sigma(\mathbf{H}_{\text{init}}^{\text{cam1}}), \mathbf{H}_{\text{cam1}}^{\text{cam2}}, \sigma(\mathbf{H}_{\text{cam1}}^{\text{cam2}})$,
Output: $\mathbf{H}_{\text{init}}^{\text{cam2}}, \sigma(\mathbf{H}_{\text{init}}^{\text{cam2}})$

Initialize $\mathbf{H}_{\text{save}[4\times4\times n]} \leftarrow \{\}$
for $i = 1$ **to** n **do**
  $\mathbf{H}(i)_{\text{init}}^{\text{cam1}} \sim \mathcal{N}(\mathbf{H}_{\text{init}}^{\text{cam1}}, \sigma(\mathbf{H}_{\text{init}}^{\text{cam1}}))$
  $\mathbf{H}(i)_{\text{cam1}}^{\text{cam2}} \sim \mathcal{N}(\mathbf{H}_{\text{cam1}}^{\text{cam2}}, \sigma(H_{\text{cam1}}^{\text{cam2}}))$
  $\mathbf{H}(i)_{\text{init}}^{\text{cam2}} \leftarrow \mathbf{H}(i)_{\text{init}}^{\text{cam1}} \cdot \mathbf{H}(i)_{\text{cam1}}^{\text{cam2}}$
  $\mathbf{H}(i)_{\text{save}} \leftarrow \mathbf{H}(i)_{\text{init}}^{\text{cam2}}$
end for
$\mathbf{H}_{\text{init}}^{\text{cam2}}, \sigma(\mathbf{H}_{\text{init}}^{\text{cam2}}) \leftarrow mean(\mathbf{H}_{\text{save}}), \sigma(\mathbf{H}_{\text{save}})$

The above algorithm describes how uncertainties are propagated from one camera to another. We begin by generating multiple realizations of the initial transformation matrix $\mathbf{H}_{\text{init}}^{\text{cam1}}$, incorporating random deviations based on its standard deviations. We do the same for the transformation between the two cameras, $\mathbf{H}_{\text{cam1}}^{\text{cam2}}$. By combining these transformations for each iteration, we compute the transformation for the second camera relative to the initial coordinate system, $\mathbf{H}_{\text{init}}^{\text{cam2}}$. Repeating this process n times allows us to derive a distribution of possible transformations, which can then be analyzed to determine the mean transformation and its associated uncertainty.

Uncertainty Propagation Forward Intersection We define a point $\mathbf{P}_{\text{init}}$ in space, along with the camera positions $\mathbf{P}_{\text{cam1}}$ and $\mathbf{P}_{\text{cam2}}$, to estimate the uncertainty of a spatial measurement. We calculate the rotation matrices $\mathbf{R}_{\mathbf{P}_{\text{cam1}}}^{\mathbf{P}_{\text{init}}}$ and $\mathbf{R}_{\mathbf{P}_{\text{cam2}}}^{\mathbf{P}_{\text{init}}}$ to align the point directly along the line of sight of each camera. These camera positions and rotation matrices define the complete transformation matrices for each camera, $\mathbf{H}_{\text{cam1}}^{\mathbf{P}_{\text{init}}}$ and $\mathbf{H}_{\text{cam2}}^{\mathbf{P}_{\text{init}}}$.

The image coordinate system follows a right-handed convention, with the origin located at the center of the image. Since the cameras are directly aligned with the point, it lies precisely on the optical axis, resulting in pixel measurements of $p_x = 0$, $p_y = 0$. We generate Monte Carlo poses using the uncertainties in the camera poses, $\sigma(\mathbf{H}_{\text{init}}^{\text{cam1}})$ and $\sigma(\mathbf{H}_{\text{init}}^{\text{cam2}})$. We determine the corresponding points in 3D space using forward intersection based on the direct linear transformation method (Hartley and Zisserman, 2004), resulting in a distribution that reflects the uncertainty in $\mathbf{P}_{\text{init}}$.

The following pseudocode outlines the procedure for propagating uncertainties through forward intersection:

Input: $\mathbf{P}_{\text{init}}, \mathbf{P}_{\text{cam1}}, \mathbf{P}_{\text{cam2}}, \sigma(\mathbf{H}_{\text{init}}^{\text{cam1}}), \sigma(\mathbf{H}_{\text{init}}^{\text{cam2}})$
Output: Set of forward intersections $\mathbf{P}_{set}$
Compute $\mathbf{R}_{\mathbf{P}_{\text{cam1}}}^{\mathbf{P}_{\text{init}}}$ from $\mathbf{P}_{\text{cam1}}$ and $\mathbf{P}_{\text{init}}$
Compute $\mathbf{R}_{\mathbf{P}_{\text{cam2}}}^{\mathbf{P}_{\text{init}}}$ from $\mathbf{P}_{\text{cam2}}$ and $\mathbf{P}_{\text{init}}$
Compute $\mathbf{H}_{\text{cam1}}^{\mathbf{P}_{\text{init}}}$ from $\mathbf{R}_{\text{cam1}}^{\mathbf{P}_{\text{init}}}$ and $\mathbf{P}_{\text{cam1}}$
Compute $\mathbf{H}_{\text{cam2}}^{\mathbf{P}_{\text{init}}}$ from $\mathbf{R}_{\text{cam2}}^{\mathbf{P}_{\text{init}}}$ and $\mathbf{P}_{\text{cam2}}$
$p_{x\,\text{cam1}}, p_{y\,\text{cam1}} \leftarrow 0, 0$
$p_{x\,\text{cam2}}, p_{y\,\text{cam2}} \leftarrow 0, 0$
Initialize $\mathbf{P}_{set} \leftarrow \{\}$
for $i = 1$ **to** n **do**
  $\mathbf{H}(i)_{\text{cam1}}^{\mathbf{P}_{\text{init}}} \sim \mathcal{N}(\mathbf{H}_{\text{cam1}}^{\mathbf{P}_{\text{init}}}, \sigma(\mathbf{H}_{\mathbf{P}_{\text{init}}}^{\text{cam1}}))$
  $\mathbf{H}(i)_{\text{cam2}}^{\mathbf{P}_{\text{init}}} \sim \mathcal{N}(\mathbf{H}_{\text{cam2}}^{\mathbf{P}_{\text{init}}}, \sigma(\mathbf{H}_{\mathbf{P}_{\text{init}}}^{\text{cam2}}))$
  $\mathbf{P}_i \leftarrow$ **forw inter***$(\mathbf{H}(i)_{\text{cam1}}^{\mathbf{P}_{\text{init}}}, \mathbf{H}(i)_{\text{cam2}}^{\mathbf{P}_{\text{init}}}, \mathbf{0})$
  $\mathbf{P}_{set} \leftarrow \{\mathbf{P}_i\}$
end for
return

forw inter* = forward intersection

3. Experiments and Results

First, we discuss the uncertainties associated with the calibration, followed by the results of the bootstrapping. Then, we integrate these uncertainty analyses into a Monte Carlo simulation and present the results for a realistic scenario.

3.1 Calibration Camera-Camera

To estimate the calibration uncertainty for the simulation, we generated test data using a system comprising two CrashCam-MINI 3530 cameras (Figure 2). The system is equipped with a 12.5 mm focal length lens for the outward-facing camera and an 8 mm focal length lens for the inward-facing camera. Each camera features a sensor with a resolution of 2560 x 1440 pixels.

The intrinsic parameters of the cameras were pre-calibrated using a test pattern, with distortion parameters - including radial and tangential distortion — estimated according to the OpenCV model. Once the pre-calibration was complete, the intrinsic parameters were excluded from the bundle adjustment to focus on optimizing the relative position and orientation of the cameras.

After pre-calibration, 140 time-synchronized images were captured for each camera while the system was moved through all six degrees of freedom. A bundle adjustment was performed using these images, with SIFT features and elliptical markers for feature detection and matching, utilizing the COLMAP software (Schönberger and Frahm, 2016), (Schönberger et al., 2016) for processing. The image block was scaled using a 2-meter reference scale with attached elliptical markers, which was 10 times larger than the baseline distance between the two cameras, providing robust scaling accuracy. The coordinate system was arbitrarily positioned in space, as only the scaling was crucial for this analysis.

The following Figure 6 illustrates the camera positions in red and the laboratory tie points in color.

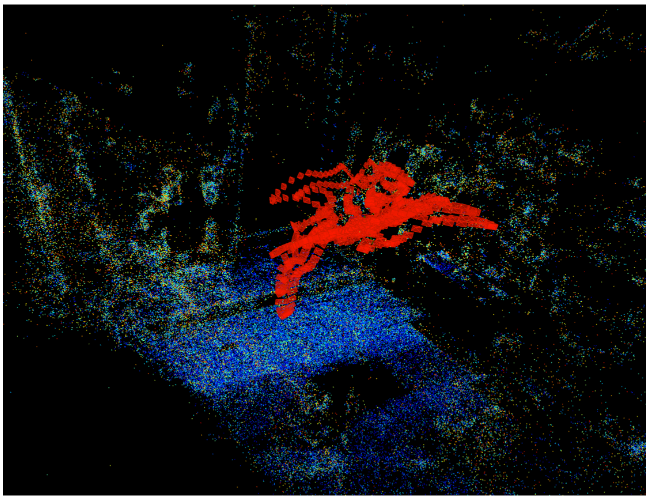

Figure 6. The camera positions are shown in red and the tie points are colored according to uncertainty. Points with a reprojection error of less than 1 pixel are represented by dark blue dots, whereas points with a reprojection error exceeding 2 pixels are indicated by red dots.

To determine the calibration parameters, we set the origin of the coordinate system at the projection center of camera 1, with the axes following the image coordinate system of camera 1 according to the OpenCV convention. The six calibration parameters for each epoch can then be determined as Equation 1.

Table 1 presents the results of the base calibration. The standard deviation of the measurement in each coordinate is approximately 2 mm. With 140 epochs (n), the standard error of the mean reduces to about 0.2 mm (assuming $\sigma_{\text{mean}} = \sigma/\sqrt{n}$). However, dividing by $\sqrt{n}$ may be too optimistic, as this does not account for potential systematic effects and correlations. For example, errors in the intrinsic parameters directly affect the baseline.

	X [mm]	Y [mm]	Z [mm]
base	61.98	-1.71	179.76
σ	2.25	3.08	1.53
$\frac{\sigma}{\sqrt{n}}$	0.19	0.26	0.13

Table 1. Results of the base calibration

Table 2 presents the results of the orientation estimation.

	ω [°]	φ [°]	κ [°]
angle	179.92	-0.09	179.76
σ	0.047	0.059	0.094
$\frac{\sigma}{\sqrt{n}}$	0.004	0.005	0.008

Table 2. Results of the orientation calibration

3.2 Bootstrapping absolute orientation

In order to ascertain realistic uncertainties for the relative orientation, two sample images (see Figure 7) are evaluated. The results obtained from this process are then compared with a 100 images bundle block adjustment in which the two images are part of the overall reconstruction. We estimated the uncertainty of the relative orientation using the methodology outlined in Section 2.3.1. The uncertainty is influenced by various factors, including the camera configuration, uncertainties in the intrinsic parameters, and uncertainties related to the matches and their distributions. Although multiple sources of uncertainty are present, a preliminary estimate can be obtained through the bootstrapping approach. In Figure 7 the keypoints are shown in red and the matches in green.

Figure 7. Two pictures with the corresponding tie point matches

We performed the reconstruction process 500 times, randomly drawing matches with replacements. This repeated sampling allowed us to evaluate the uncertainty of the relative orientation in a probabilistic manner. The results for two parameters are presented in figures 8 and 9. In these figures, the dashed line represents the 1σ confidence interval. The standard deviation of the base is in the range of 2 mm, while the orientation is in the range of 0.02°. These values are assumed for the following Monte Carlo simulation.

This contribution has been peer-reviewed. The double-blind peer-review was conducted on the basis of the full paper.
https://doi.org/10.5194/isprs-annals-X-G-2025-461-2025

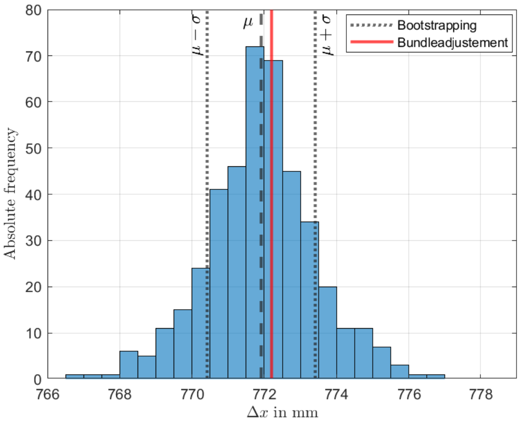

Figure 8. Translation in x-axis

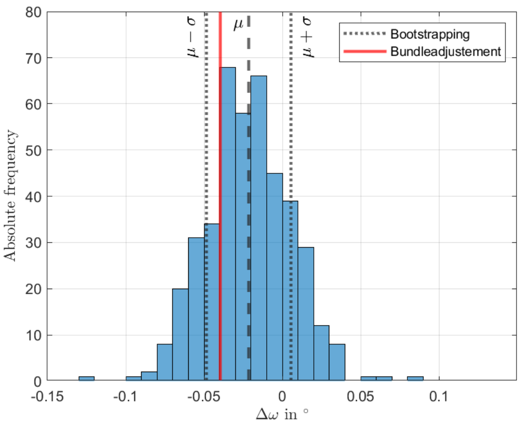

Figure 9. Orientation x-axis

3.2.1 Bundel adjustment Camera-Reference System We localized the outward-facing camera using bundle adjustment. To achieve accurate localization, it is recommended that the scene contains significant depth information, which can be measured in advance by an additional reference camera. Once this depth information is captured, we add the corresponding images of the scene to the bundle adjustment process. The intrinsic parameters of the cameras are determined in advance using a test field calibration, ensuring that lens distortion and other camera-specific characteristics are accurately modeled. The uncertainty of the bundle adjustment is subsequently calculated from the covariance matrix obtained during the optimization process. For our simulation, we assume uncorrelated observations with a standard deviation of 1 mm for positional measurements and 0.01 degrees for rotational measurements in all directions.

3.3 Monte Carlo Methods

This section discusses the Monte Carlo method, focusing on the uncertainties of the inward-facing cameras and the point measurements, including their confidence intervals.

3.3.1 Camera-Camera The first step in the uncertainty estimation process is to determine the uncertainty associated with the inward-facing camera (cam2). This is achieved using 500 poses of the outward-facing camera (cam1) and 500 inter-camera transformations (cam1 to cam2). The transformation and its associated uncertainty were determined beforehand through calibration. The poses and transformations are randomly generated and assumed to follow a normal distribution. The uncertainties are then propagated using a Monte Carlo simulation to obtain a robust estimate of the uncertainty for cam2. Once the uncertainty for cam2 is established, the uncertainty for the attached third camera (cam3) is estimated. This estimation process incorporates uncertainties derived using the bootstrapping method, which provides a robust measure of variability in the pose estimates. The uncertainties are again propagated and combined within a Monte Carlo simulation to obtain the final uncertainty estimate. The results are presented in the following tables. Table 3 reports the uncertainties in translation within the world coordinate system, while Table 4 presents the uncertainties in orientation within the world coordinate system.

	1σX [mm]	1 σ Y [mm]	1 σZ [mm]
cam 1	1.00	1.00	1.00
cam 2	1.52	1.54	1.52
cam 3	2.53	2.51	2.55

Table 3. Uncertainties of translation in the world coordinate system

	ω [°]	φ [°]	κ [°]
cam 1	0.01	0.01	0.01
cam 2	0.011	0.011	0.013
cam 3	0.023	0.023	0.024

Table 4. Uncertainties of orientation in the world coordinate system

3.3.2 Forward Intersection To estimate the uncertainty resulting from the configuration, a regular grid is placed over a realistically sized car interior. Figures 10, 11, 12, and 13 represent the car interior. This corresponds to the typical seating area of a station wagon. The cameras are positioned in realistic locations: one in the rear area, facing outward from the trunk, and another in the door area of the second row of seats.
To ensure that each point is situated within the image area, the camera is rotated directly to the point in question, thereby ensuring that the mark measurement is consistently positioned in the center of the image. The poses are generated using Monte Carlo simulation, and the associated uncertainty is calculated in a subsequent step. The points within the vehicle interior are then calculated from the poses generated in this manner (2.3.2). Each measurement point is represented as a cluster of points in the Monte Carlo simulation to account for uncertainty. The configuration and pose uncertainties are quantified by the standard deviation of this point cluster. For each spatial axis, the maximum standard deviation is assessed to determine whether it remains below the threshold of 5 mm. The maximum standard deviation across all axes is visualized using a heat map. In Figure 10, four cameras are depicted, and the uncertainties of the camera pairs are assumed to be identical. The simulated points are at the same height as the cameras in this configuration. The intersection geometry is optimal when the interior angle at the simulated point is 90 degrees and occurs when the simulated point lies on the

surface of the sphere. This sphere is defined by the center point that lies directly between the two projection centers of the cameras and the diameter as the distance between the two cameras. Consequently, the cameras are positioned directly on this spherical surface. The optimal internal angle is visible here as a dark green semicircle in the figure. Directly between the cameras, the interior angle approaches 180 degrees, which results in the simulated directions intersecting the point very obliquely. This causes the confidence ellipse to be strongly distorted in this direction, making it impossible to measure points with an uncertainty of less than 5mm.

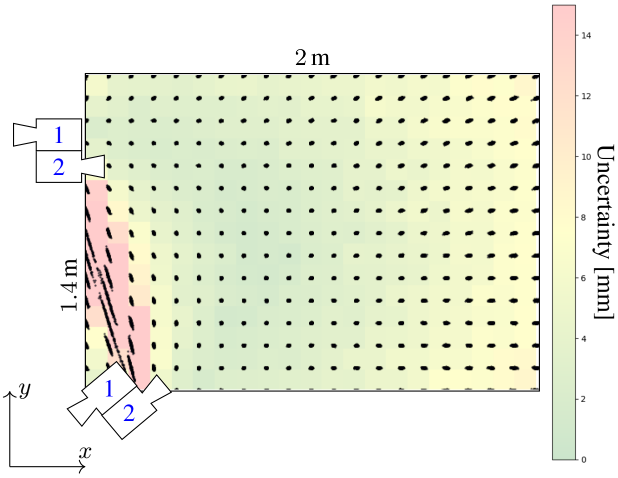

Figure 10. Four camera system points at the same height

Figure 11 describes the same configuration, but with the simulated points positioned 30 cm higher than the cameras. As a result, the optimal intersection geometry shifts more toward the cameras due to the intersection on the sphere’s surface. The intersection geometry directly between the cameras improves because they now point upwards, reducing the interior angle and enhancing measurement reliability.

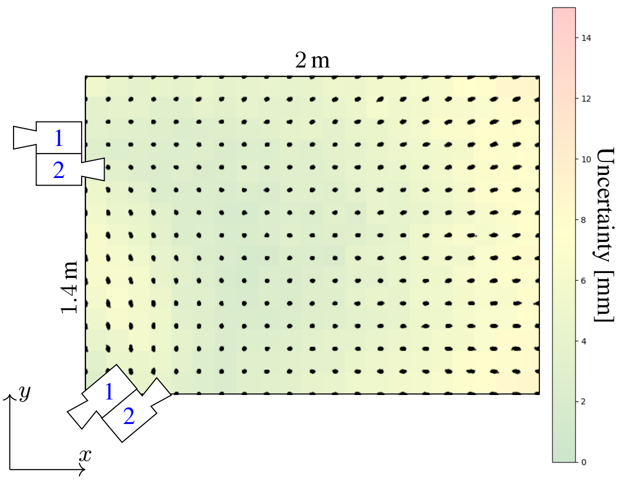

Figure 11. Four camera system points at locations 30 cm higher

Figure 12 describes a configuration with an outward-facing camera and a connected absolute orientation camera (cam 3). In this analysis, uncertainties related to the scale measurement and the potential deformation of the scale during the experiment are neglected here. In this configuration, it is predominantly possible to achieve measurements with a standard deviation of less than 5 mm in all spatial directions. The uncertainty of the point measurement is lower near the attached camera, as the influence of the camera’s angle measurement is reduced in that area.

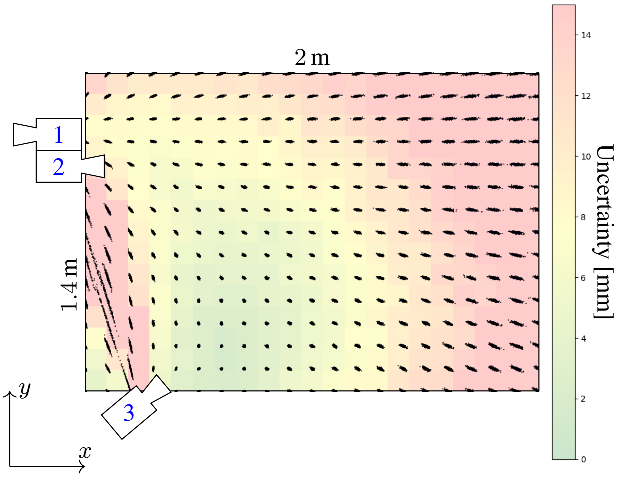

Figure 12. Three camera system points at the same height

Figure 13 once again demonstrates the impact of a 30 cm height shift on the plane. It is evident that the uncertainties increase significantly in the rear area, while the intersection geometry between the cameras becomes less challenging, resulting in a smaller standard deviation.

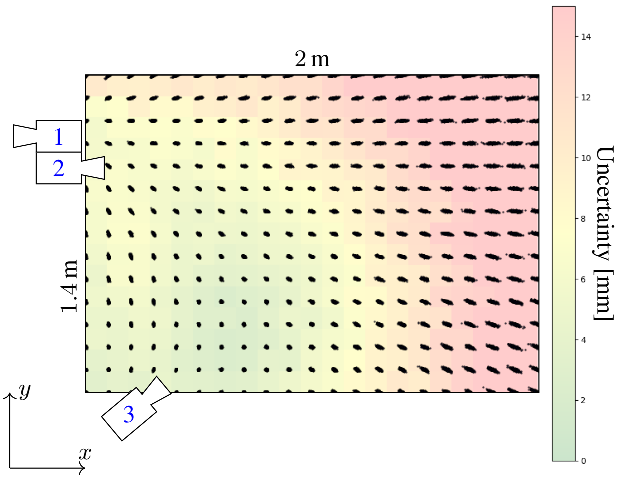

Figure 13. Three camera system points at locations 30 cm higher

However, camera uncertainties can vary considerably based on the overlap region among cameras, and in some areas, localization may be impossible. Furthermore, potential correlations between parameters and measurements, as well as the uncertainties associated with the markers themselves, have not been accounted for. Despite these considerations, simulations showed that point uncertainties below 5 mm are achievable with the current camera configuration. In a three-camera setup, the measurement point should ideally be placed closer to camera 3, since its orientation is less precisely determined compared to camera 2. Minimizing the distance to camera 3 therefore remains essential for accurate measurements.

4. Conclusions

An alternative outward-facing camera approach was proposed to circumvent the challenges of direct localization inside the vehicle. Key uncertainties were identified and incorporated into a Monte Carlo simulation. Given the large number of parameters, further in-depth analyses are necessary. In particular, the correlations omitted here should be thoroughly examined in future studies. Nonetheless, the geometry formed by the cameras and the measurement point continues to be a primary driver of measurement accuracy. By combining uncertainty analyses—derived from real data and evaluated through bootstrapping—within a Monte Carlo framework, regions were identified where an uncertainty level below 5 mm can be attained under specified conditions. This degree of accuracy aligns well with crash test requirements, indicating significant potential for practical use in studying kinematics within the vehicle interior. To enhance the robustness of the system, future work could involve integrating data from acceleration and angular rate sensors. Additional avenues for research include increasing the number of observations, modeling points in the interior, and incorporating potential influences from pre-simulations.

References

Björkholm, P., Landén, L., Stigwall, J., Johannisson, P., Södermalm, S., Andersson, P., Johnsson, C., 2010. Navigation in vehicle crash test using mems-based imu. *IEEE/ION Position, Location and Navigation Symposium*, 27–31.

Butz, I., Moser, S., Nau, S., Hiermaier, S., 2021. Data assimilation of structural deformation using finite element simulations and single-perspective projection data based on the example of X-ray imaging. *SN Applied Sciences*, 3(5), 545.

Efron, B., 1979. Bootstrap methods: another look at the jackknife. *The Annals of Statistics*, 7(1), 1–26. Institute of Mathematical Statistics.

Hartley, R. I., Zisserman, A., 2004. *Multiple View Geometry in Computer Vision*. Second edn, Cambridge University Press.

Leost, Y., Nakata, A., Bösl, P., Butz, I., Soot, T., Kurfiß, M., Moser, S., Kase, F., Hashimoto, T., Shibata, S., 2020. An engineering approach of an x-ray car crash under reverse small overlap configuration.

Metropolis, N., Ulam, S., 1949. The Monte Carlo method. *Journal of the American Statistical Association*, 44(247), 335–341. Taylor & Francis.

Raguse, K., Heipke, C., 2009. Synchronization of Image Sequences - A Photogrammetric Method. *Photogrammetric Engineering & Remote Sensing*, 75.

Schönberger, J. L., Frahm, J.-M., 2016. Structure-from-Motion Revisited. *Conference on Computer Vision and Pattern Recognition (CVPR)*.

Schönberger, J. L., Zheng, E., Pollefeys, M., Frahm, J.-M., 2016. Pixelwise View Selection for Unstructured Multi-View Stereo. *European Conference on Computer Vision (ECCV)*.

Zhang, W., Furukawa, T., Nakata, A., Hashimoto, T., 2022. Localization of Stereovision for Measuring In-Crash Toeboard Deformation. *Sensors*, 22(8), 2962.